Hindawi
Shock and Vibration
Volume 2020, Article ID 8885905, 9 pages
https://doi.org/10.1155/2020/8885905

Research Article

Mechanical Model of the Initial Leg Pressure Increment of the Shield and Its Application to Monitor Roof Load in Longwall Panels

Like Wei [1,2,3]

[1]*State Key Laboratory of Coal Mine Disaster Dynamics and Control, Chongqing University, Chongqing 400044, China*
[2]*College of Resource and Safety, Chongqing University, Chongqing 400044, China*
[3]*Information Research Institute, Ministry of Emergency Management, Beijing 100029, China*

Correspondence should be addressed to Like Wei; wlkyo@qq.com

Received 13 September 2020; Revised 8 October 2020; Accepted 19 October 2020; Published 30 October 2020

Academic Editor: Chen Miao

The shield pressure cannot always be used to represent the upper load of longwall panels, since its value is steady or even decreases by the yielding action. However, the leg pressure increment of the shield (LPIS) at the initial stage is not influenced by yielding and could therefore be an important factor to judge the state of overlying loads. In this study, a mechanical model is established to analyze the relationship between the overlying loads of the main roof and LPIS after cutting. There is a linear positive correlation between leg pressure increment and overlying loads and a second-order relationship between leg pressure increment and length of main roof cantilever in the proposed model. Therefore, it can be used to determine the magnitude of roof weighting strength in different periods as well as the length of the main roof cantilever in a period. Finally, the mine pressure difference between the period of fully mechanized mining and the period of fully mechanized caving mining in the MinDong-1 coal mine serves to verify the rationality of the proposed model.

1. Introduction

Longwall mining plays a predominant role in coal mining in China, owing to its high-efficiency superiority in coal production [1, 2]. Various theories have been proposed to interpret the shield-roof interaction as well as determining the shield capacity in longwall mining for decades [3, 4], such as the classical theory of key blocks in the voussoir beam structure in longwall mining [5], "Roof-support-floor" system model for steeply dipping seam mining [6], overburden structure for thick coal seam mining [7], the upper and lower step rock beams, and the upper masonry beam-the lower step rock beam and the upper masonry beam-the lower masonry beam for shallow buried coal seam mining [8]. Moreover, the shield's load capacity also increases along with the increase of the panel production and automation, as reported by the case in Shangwan mine located in Inner Mongolia. It presently reaches 26,000 kN and has resulted in an increase in the diameter of the shield leg [9]. Nevertheless, high capacity of the shield and the aforementioned theories cannot solve all the issues in the longwall panel. Disasters such as shield crushing [10, 11] and rockburst [12] still occur during the retreating of some panels due to complex engineering-geological conditions.

To address the above issues, field monitoring in longwall panels is necessary to prevent these disasters. An intelligent monitoring-analysis system for coal mine rockburst hazard has been developed currently by the National Coal Mine Safety Administration in China [13]. Due to the unpredictability and suddenness of rock burst, the use of one single method is not enough to monitor the shock behavior on the roadway and to study the bursting failure process at the excavation area [14]. Thus, multisource information [15] is used to detect upper loads and failure processes of the surrounding rock in longwall panels and to improve the reliability of monitoring results, where the multisource

information is based on real-time data from microseism, acoustic emission, electromagnetic radiation monitoring, and shield pressure monitoring. Previous studies have revealed that the upper concentrated load of the mining engineering structure is the most important and critical factor for rockburst [16]. However, the methods monitoring the upper concentrated load of longwall panels heavily rely on microseismic monitoring [17–21]. However, shield pressure monitoring is rarely reported.

Shield pressure could be an effective factor to represent the upper loads of longwall panels, but its value is either steady or decreases with yielding as shown in Figure 1 (stage C). In order to use the shield pressure data effectively, we can analyze both the period before yield valves opening (stage A) and the period of shield pressure increase (stage B) in Figure 1. In recent years, Cheng [22] has calculated the leg pressure increment of approximately 32000 shield supporting cycles and found a powerful connection between the magnitude of the leg pressure increment and the periodic roof weighting. Thus, the leg pressure increment of the shield (LPIS) can be used as an index to evaluate the interaction between shields and the roof and to identify the periodic weighting. In this paper, LPIS after shield setting is used to establish an LPIS model based on a simplified shield-roof interaction model which interprets the relationship between roof loads and LPIS. Finally, according to the field observations, the LPIS model feasibility is verified during the period ranging from fully mechanized mining to fully mechanized caving mining. Results from the proposed LPIS model and some other monitoring approaches in longwall panels can support each other.

2. Mechanical Model of LPIS

2.1. LPIS Model Foundation. The shield-roof interaction model is proposed in order to find the relationship between roof loads and the LPIS. Considering that various mechanical properties will affect the distribution of support pressure, therefore, this model cannot be applied in the real-time analysis due to the fact that some parameters cannot be acquired in real time. To build a practical model, the field structure around longwall panels should be simplified, retaining the key and easily obtained factors. In this paper, the main roof, the immediate roof, the coal seam, and the shield are all included in the engineering structure, as shown in Figure 2.

Many scholars have analyzed the main roof by considering the support pressure relationship between the coal seam and the immediate roof to be elastic [23–26]. Based on this, some basic results such as the deflection solution for the main roof and the maximum bending moment in the front of a coal wall can be obtained. To simplify the analysis, the above assumption is also accepted in this paper. Besides, the overlying load of the main roof is regarded as a local uniform load while the force of shield acting on the main roof is simplified as a point load. Thus, a shield-roof interaction model before and after cutting is shown in Figure 3.

The main roof can be regarded as a cantilever. The deflection of the point shield acting before cutting is defined as follows:

$$W_1 = \frac{QL_S^2}{24EI}\left(L_S^2 - 4L_CL_S + 6L_C^2\right) - \frac{PL_S^3}{3EI}, \tag{1}$$

where Q is the overlying load of the main roof, L_S is the distance between the point shield acting on the main roof and the coal wall, L_C is the length of the cantilever of the main roof, P is the leg pressure of the shield before cutting that acts on the main roof, E is the tensile elastic modulus of the main roof, and I is the moment of inertia of the main roof, as shown in Figure 3(a).

Deflection of the point shield after cutting (Figure 3(b)) can be expressed as follows:

$$W_2 = \frac{Q(L_S+d)^2}{24EI}\Big((L_S+d)^2 - 4(L_C+d)(L_S+d) + 6(L_C+d)^2\Big) - \frac{(P+\Delta P)(L_S+d)^3}{3EI}, \tag{2}$$

where d is shearer's cutting distance and ΔP is the leg pressure increment of the shield after cutting as shown in Figure 3(b). Thus, the leg pressure of the shield which acts on the main roof becomes $P + \Delta P$. The length of the main roof cantilever changes to $L_C + d$ while the distance between the point shield acting on the main roof and the coal wall becomes $L_S + d$.

Δhis the sinkage of the point shield acting on the main roof. It can be expressed by the difference between the deflection of the point shield before and after cutting, as follows:

$$\Delta h = W_2 - W_1. \tag{3}$$

The main roof can be assumed to be a rigid body due to its thickness and hardness [3]. Thus, the relationship among the sinkage of the immediate roof, the compression of the shield, and the compression of the floor is defined as follows:

$$\Delta h_r + \Delta h_s + \Delta h_f = \Delta h, \tag{4}$$

where Δh_r is the sinkage of the immediate roof; Δh_s is the compression of the shield, and Δh_f is the compression of the floor as shown in Figure 4.

The equilibrium condition of forces for the sinkage model of the floor-shield-roof can be defined as follows:

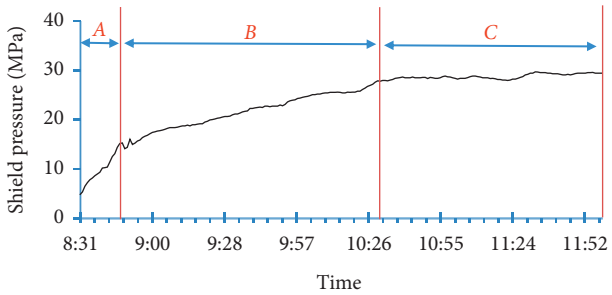

Figure 1: Real supporting load variation after the initial setting in a typical cycle.

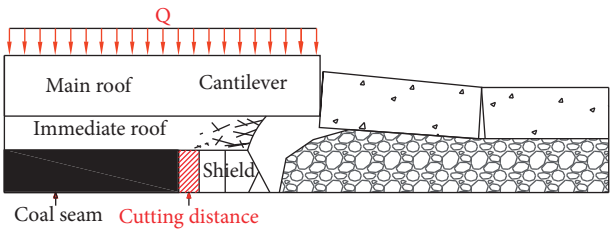

Figure 2: Engineering structure around Longwall Panel.

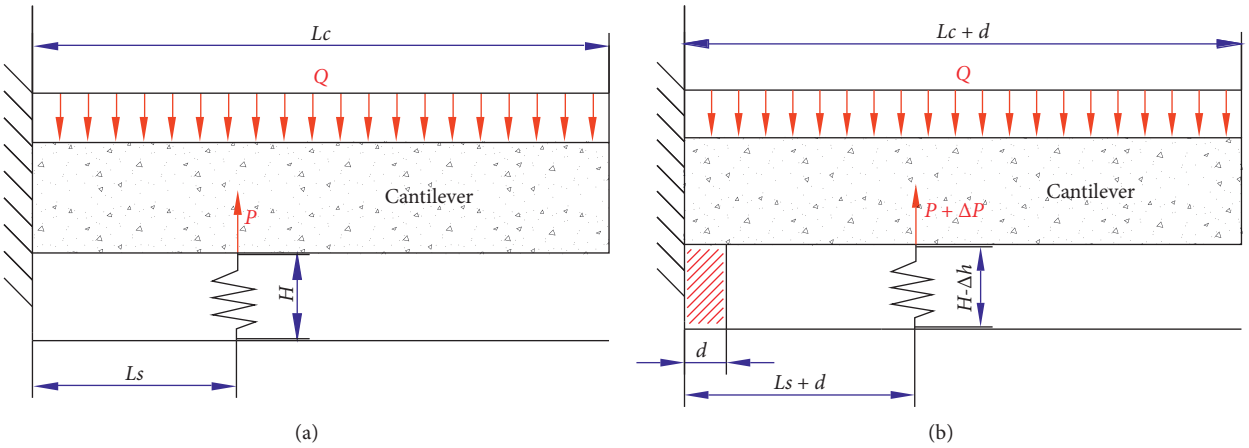

Figure 3: Shield-roof interaction model. (a) Before cutting. (b) After cutting.

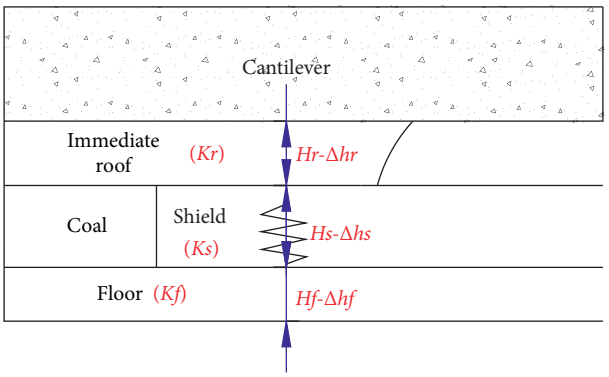

Figure 4: Sinkage model of floor-shield-roof.

$$K_r \Delta h_r = K_s \Delta h_s = K_f \Delta h_f = \Delta P, \tag{5}$$

where K_r is the stiffness of the immediate roof; K_s is the stiffness of the shield, and K_f is the stiffness of the floor.

A simultaneous solution for (1), (2), (3), (4), and (5) can be obtained as follows:

$$\Delta P = \frac{Q\left(12\, dL_S L_C^2 + 12d^2 L_S L_C + 6d^2 L_C^2 + 4d^3 L_S + 8d^3 L_C + 3d^4\right) - 8P\left(\left(L_S + d\right)^3 - L_S^3\right)}{24EI\left(\left(1/K_f\right) + \left(1/K_r\right) + \left(1/K_s\right)\right) + 8\left(L_S + d\right)^3}. \tag{6}$$

Therefore, the LPIS model can be described by the previous formula.

2.2. Application of the LPIS Model

2.2.1. Application of the LPIS Model for Defining the Strength of the Roof Weighting. A linear positive correlation between ΔP and Q is clearly shown in (6). Thus, the greater the leg pressure increment for the same cantilever length, the greater the corresponding overlying load of the main roof for different roof weighting periods. Meanwhile, the greater the leg pressure of the shield before cutting, the smaller the leg pressure increment. On this basis, the IPIS model can be used to estimate the strength of the roof weighting.

2.2.2. Application of the LPIS Model for Defining the Length of the Cantilever. In addition, if the overlying load of the main roof has little change, the overlying load of the main roof Q can be regarded as a constant and the LPIS model (6) can be rewritten as follows:

$$\Delta P = \frac{\left(12\, dL_S Q + 6d^2 Q\right)L_C^2 + \left(12d^2 L_S Q + +8d^3 Q\right)L_C + 4d^3 L_S Q + 3d^4 Q - 8P\left(\left(L_S + d\right)^3 - L_S^3\right)}{24EI\left(\left(1/K_f\right) + \left(1/K_r\right) + \left(1/K_s\right)\right) + 8\left(L_S + d\right)^3}. \tag{7}$$

Base on (7), there is a second-order relationship between ΔP and L_C; however, a different leg pressure of the shield P will disrupt this second-order relationship. Therefore, it is better in practice to select the same initial setting pressure to estimate the length of the cantilever L_C.

2.2.3. Application of the LPIS Model for Time Determination. In order to reasonably apply the LPIS model, the determination of time ΔP after the initial setting is very important for predicting the strength of the roof weighting and the length of the cantilever L_C. After a long computing time, it not possible to distinguish the strength of the roof weighting between period A and period B as shown in Figure 5. This is because their leg pressure increments ΔP are equal if we select time T1 for computing. However, the strength of the roof weighting in period A is obviously stronger than that in period B since ΔP_A is greater than ΔP_Bbased on the LPIS model when time T2 is selected for computing. On the other hand, a very short computing time will lead to other unpredictable factors influencing the results and in particular ΔP. Consequently, an appropriate determination of the computing time should be shorter than the shortest time from the initial setting to yield value open in previously normal period, so that it is possible to find the abnormal strength of the roof weighting.

3. Measuring the Roof Load Using on the LPIS Model

3.1. Engineering Background. The MinDong-1 coal mine is located in the northeast of the Inner Monggol Autonomous Region in China as shown in Figure 6. Its designed annual production capacity is 5 Mt, and the recoverable reserve is approximately 7 billion tons. The key minable seam is the 16–3 coal seam and mined firstly. The characteristics of the coal seams are described in Table 1. The average thickness of the 16–3 coal seam is 9.7 m, but the designed cutting height is only 3 m, and the rest is mined through caving. The abundance of water in the overlying strata is explained by the hydrological condition described in Table 1. It can be seen that water is very abundant between the 16–2 coal seam and the 16–3 coal seam, and especially in overlying strata of the 16–3 coal seam.

Due to the complex hydrological condition, a water inrush accident occurred in the I0116-3-01 working face (the first longwall panel in the 16–3 coal seam) and caused one casualty. At that time, the water inflow in the I0116-3-01 working face reached up to 950 m^3/h. After the accident, the fully mechanized top-caving mining was replaced by the general fully mechanized mining to ensure more safety. Consequently, two different types of roof loads would be suitable to use for verifying the LPIS model.

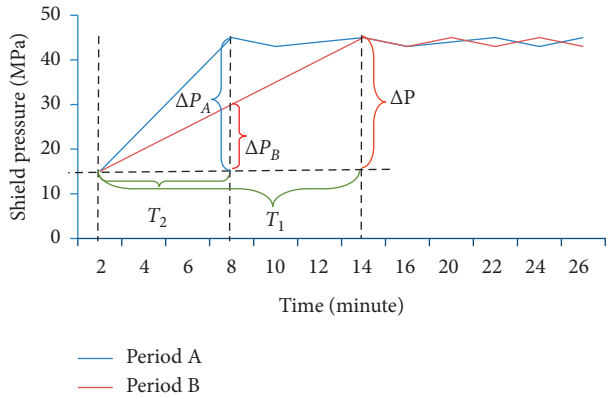

Figure 5: Supporting load variation after the initial setting in two periods.

Figure 6: Location of MinDong-1 coal mine.

The width of the I0116-3-01 working face in the 16–3 coal seam is 197.5 m. It has a ZF9000/17/32-type shield and a working resistance of 9,000 kN (36.56 MPa). Both legs of each shield are equipped with hydraulic pressure transducers that are capable of collecting and storing data. Before the water inrush disaster occurred, ten transducers were installed on shields 12#, 24#, 36#, 48#, 60#, 72#, 84#, 96#, 108#, and 120#, respectively. For analyzing the influence

Table 1: Position relation of coal seams.

Lithology	Stratum thickness (m)	Depth (m)	Hydrological condition
Conglomerate	39.50	225.85	The water-abundance is moderate, the unit water inrush q varies from 1.06 (L/s.m) to 6.90 (L/s.m), and the permeability coefficient K varies from 1.26 (m/d) to 8.33 (m/d).
Siltstone	10.85	236.70	
Mudstone	4.60	236.70	
16–2 coal seam	1.50	238.20	
Mudstone	3.40	241.60	
Siltstone	8.95	250.55	
Fine sandstone	5.75	256.30	The water-abundance is high, the unit water inrush q varies from 0.15 (L/s.m) to 1.38 (L/s.m), and the permeability coefficient K varies from 0.28 (m/d) to 1.71 (m/d).
Conglomerate	7.10	263.40	
Siltstone	8.20	271.60	
Mudstone	1.70	273.30	
Siltstone	8.25	281.55	
16–3 coal seam	9.70	291.25	
Fine sandstone	2.9	294.15	
Siltstone	5.95	300.1	

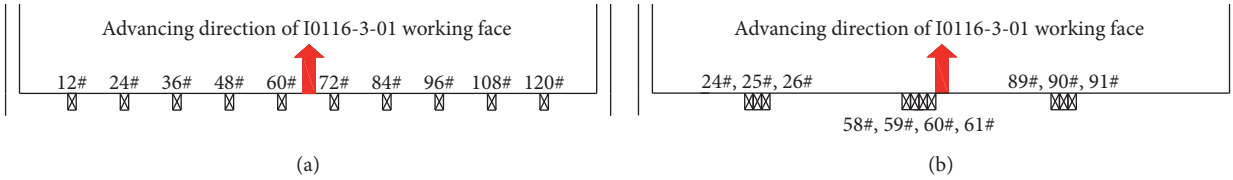

Figure 7: Installation location of transducers. (a) Before water inrush disaster. (b) After water inrush disaster.

of neighboring shields, transducer locations were changed as shown in Figure 7.

3.2. Field Application of the LPIS Model. Based on the LPIS model built in Chapter 2.1, the strength of the roof weighting and the cantilever length can be represented by the application method in 2.2. Besides, choosing the proper time ΔP after the initial setting is extremely essential with regard to field application, while an increasing time shorter than the shortest time from the initial setting to the previous normal period yield value should be appropriate.

For further data analysis, the middle parts of shields from 58# to 61# are considered representative of the whole longwall panel because the roof weighting is the strongest in that area. The leg pressure increment is calculated as the average value of both legs of each shield, and the increasing time is 10 minutes based on the historical data of shield pressures. The frequency of data sampling is minute-based depending on the manufacturer of hydraulic pressure transducers. The fully mechanized caving mining was started again after performing the control technology for water disaster. Thus, the pressure data during the periods of fully mechanized mining and fully mechanized caving mining were recorded. The relationship between the leg pressure increment and the distance of progression in both periods is described in Figure 8.

Figure 8(a) displays leg pressure increment changes between 508 m and 568 m; meanwhile, the variation between 719 m and 779 m is shown in Figure 8(b). The peak value of the leg pressure increment during the fully mechanized mining period is approximately equal to 10 MPa and much greater than the peak value of the leg pressure increment during the fully mechanized caving mining period which is lower than 8 MPa. Generally, the strata pressure during the fully mechanized mining period is stronger than that during the fully mechanized caving mining period, and mine pressure is lower when the coal seam is thicker [27]. Therefore, the magnitude of the leg pressure increment ΔP can represent the strength of the strata pressure based on the results from the LPIS model.

4. Discussion

As mentioned above, it was possible to successfully predict the strength of the roof weighting using the LPIS model in the MinDong-1 coal mine. A positive correlation between the overlying load of the main roof and the leg pressure increment of the shield after cutting is obvious. However, a second-order relationship between the LPIS after cutting and the length of the main roof cantilever was less evident. That phenomenon may be caused by two-dimensional and three-dimensional factors which influence the LPIS model.

4.1. Two-Dimension Influence Factor of LPIS Model. The reason for a less evident second-order relationship might be the disturbance due to different initial setting pressures. Although we theoretically suggest selecting the same initial setting pressure to estimate the length of the cantilever in Chapter 2.2, it appeared that the initial setting pressure actually had various values influenced by field operations.

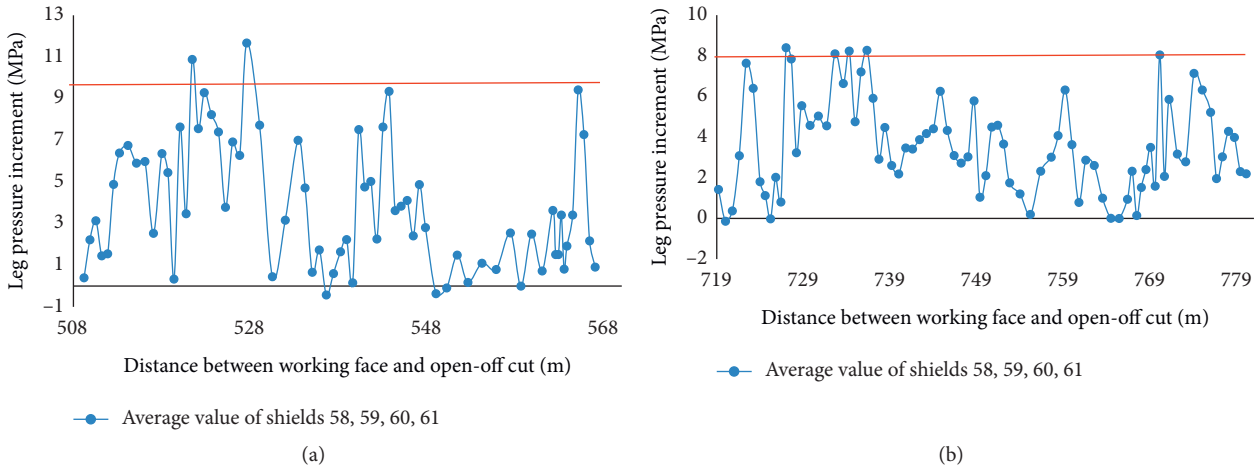

Figure 8: The relationship between leg pressure increment and distance of progression. (a) Period in fully mechanized mining. (b) Period in fully mechanized caving mining.

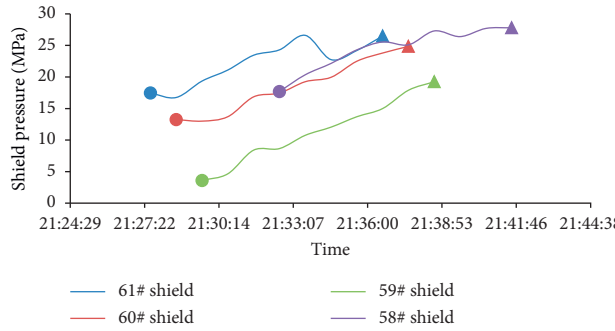

Figure 9: Four neighboring supporting loads variation after the initial setting in the same period.

Taking the field data of one period, for example, four different variation curves are obtained as shown in Figure 9 for neighboring shields from 58 to 61. In the figure, the circular points refer to the initial setting pressure while the triangular points correspond to the pressure after ten minutes.

For analyzing the characteristics of the four curves, more detailed information including the initial setting time, the initial setting pressure, the pressure after ten minutes, and the leg pressure increment are shown in Table 2.

It is obvious that for a greater initial setting pressure, the pressures after ten minutes for shields 58# to 61# are higher. However, the greater the initial setting pressure, the lesser the leg pressure increment for shields 59# to 61#. There is an abnormal phenomenon observed in shields 58# to 61#. In fact, it has been noted that the leg pressure increment for an initial setting pressure of 17.45 MPa is lower than the leg pressure increment for an initial setting pressure of 17.7 MPa. Therefore, the difference in the initial setting pressure is not the unique influencing factor of the LPIS model.

4.2. Three-Dimension Influence Factor of LPIS Model. Cheng [16] showed that there is a factor influencing the LPIS model in a three-dimension condition. The shield pressure increment and the distance from the shield to the front drum have the following relationship:

$$y = \frac{\Delta L}{1 + \Delta L p e^{x \ln q}}, \tag{8}$$

where ΔL is the relatively stable leg pressure increment value and p and q are constants.

Thus, different positions of the shear after the initial setting will also disrupt the normal vibration of the shield pressure increment. Besides, based on field data shown in Table 3, it was found that an irregular progress time will lead to an abnormal pressure increment of neighboring shields. The initial setting time of shield 61# is much earlier than that of neighboring shields, and the leg pressure increment of the shield is much greater than others. Due to the slow progress, the leg pressure increments of shields 58# to 60# remained almost unchanged after the initial setting.

In conclusion, the two-dimensional and three-dimensional conditions mentioned above should be similar if we want to effectively exploit the LPIS model. The development of an intelligent mining workface will help us control the above conditions, and the model will hopefully be successfully applied to an intelligent mining workface in the future.

Table 2: Typical difference in leg pressure increment in the same period.

Shield number	61	60	59	58
Initial setting time	21 : 27	21 : 28	21 : 29	21 : 32
Initial setting pressure (MPa)	17.45	13.25	3.6	17.7
Pressure after ten minutes (MPa)	26.5	24.85	19.25	27.8
Leg pressure increment (MPa)	9.05	11.6	15.65	10.1

Table 3: Typical difference in leg pressure increment in the same period.

Shield number	61	60	59	58
Initial setting time	2 : 48	2 : 52	2 : 52	2 : 56
Initial setting pressure (MPa)	13.45	26.3	26.05	27.55
Pressure after ten minutes (MPa)	21.65	26.25	25.8	27.55
Leg pressure increment (MPa)	8.25	−0.05	−0.25	0

5. Conclusion

The results obtained in this study lead to the following conclusions:

(1) The shield pressure cannot always represent the upper load of longwall panels because its value depends on the yielding effect; however, the leg pressure increment of the shield is an important factor that can be used to analyze the main roof.

(2) The LPIS model has been built to establish the linear positive correlation between the overlying load of the main roof and the leg pressure increment of the shield after cutting. This can be used to determine the magnitude of the roof weighting strength during different periods as well as the cantilever length of the main roof.

(3) The LPIS model was applied to the MinDong-1 coal mine for predicting the strength of the roof weighting. A satisfying performance of the model was proved by comparing shield pressure data during both fully mechanized mining and fully mechanized caving mining periods. The peak value of the leg pressure increment of the shield during different periods also served to demonstrate the reliability of the model.

Data Availability

The data used to support the findings of this study are included in the article.

Conflicts of Interest

The author declares no conflicts of interest.

Acknowledgments

This work was supported by the National Nature Science Foundation of China (no. 52004243) and the National Key Research and Development Plan (2017YFC0804202) which are gratefully acknowledged.

References

[1] Y. Ji, T. Ren, P. Wynne, Z. Wan, Z. Ma, and Z. Wang, "A comparative study of dust control practices in Chinese and Australian longwall coal mines," *International Journal of Mining Science and Technology*, vol. 26, no. 2, pp. 199–208, 2016.

[2] J. Fan, P. Liu, J. Li, and D. Jiang, "A coupled methane/air flow model for coal gas drainage: model development and finite-difference solution," *Process Safety and Environmental Protection*, vol. 141, no. 9, pp. 288–304, 2020.

[3] M. G. Qian, X. X. Miao, J. L. Xu et al., *Theory of Key Strata in Ground Control*, China University of Mining and Technology Press, Xuzhou, China, 2003.

[4] C. Shu, J. Fan, H. Wang, P. Liu, and Y. Xu, "Temperature variations of coal in the heading face measured using a thermo-hydro-mechanical model considering desorptional heat," *Applied Thermal Engineering*, vol. 181, no. 11, Article ID 115969, 2020.

[5] M. G. Qian, X. X. Miao, and F. L. He, "Analysis of key block in the structure of voussoir beam in longwall mining," *Journal of China Coal Society*, vol. 31, no. 6, pp. 557–563, 1994.

[6] Y. P. Wu, "Dynamic model and stability of system "roof support-floor" in steeply dipping seam mining," *Journal of China Coal Society*, vol. 29, no. 5, pp. 527–531, 2004.

[7] B. Yu, J. X. Yang, C. Y. Liu, and R. Gao, "Study on overburden structure and mechanism of rock pressure in large space stope," *Journal of China Coal Society*, vol. 44, no. 11, pp. 3295–3307, 2019.

[8] K. J. Huang, Q. X. Huang, S. J. Wang, Z. S. Deng, and M. Y. ZHAO, "Research on roof structure and support resistance during periodic weighting in shallow group coal seams mining face," *Journal of China Coal Society*, vol. 43, no. 10, pp. 2687–2693, 2018.

[9] J. Y. Cheng, Z. J. Wan, and Y. L. Ji, "Shield-roof interaction in longwall panels: insights from field data and their application to ground control," *Advances in Civil Engineering*, vol. 2018, Article ID 3031714, 18 pages, 2018.

[10] C. Liu, Z. Q. Yang, P. L. Gong et al., "Accident analysis in relation to main roof structure when longwall face advances toward a roadway: a case study," *Advances in Civil Engineering*, vol. 2018, Article ID 3810315, 11 pages, 2018.

[11] H. Kang, H. Lv, X. Zhang, F. Gao, Z. Wu, and Z. Wang, "Evaluation of the ground response of a pre-driven longwall recovery room supported by concrete cribs," *Rock Mechanics and Rock Engineering*, vol. 49, no. 3, pp. 1025–1040, 2016.

[12] Q. X. Qi, Z. Yi, S. K. Zhao et al., "Seventy years development of coal mine rockburst in China: establishment and consideration of theory and technology system," *Coal Science and Technology*, vol. 47, no. 9, pp. 1–41, 2019.

[13] L. K. Wei, D. Y. Jiang, C. Wang, J. Chen, S. Gao, and J. Y. Fan, "Key technology architecture of the intelligent monitoring-analysis system for coal mine rockburst hazard risk supervision," *Journal of China Coal Society*, 2020.

[14] J. Fan, J. Chen, D. Jiang et al., "A stress model reflecting the effect of the friction angle on rockbursts in coal mines," *Geomechanics and Engineering*, vol. 18, no. 1, pp. 21–27, 2019.

[15] R. S. Jia, X. H. Yan, H. M. Sun, J. C. Fan, H. B. Yang, and C. F. Wu, "Situation assessment method of rock burst based on multi-source information fusion," *Journal of Mining & Safety Engineering*, vol. 31, no. 2, pp. 187–195, 2014.

[16] H. P. Kang, G. Xu, B. M. Wang et al., "Forty years development and prospects of underground coal mining and strata control technologies in China," *Journal of Mining and Strata Control Engineering*, vol. 1, pp. 1–33, 2019.

[17] C. Srinivasan, S. K. Arora, and S. Benady, "Precursory monitoring of impending rockbursts in Kolar gold mines from microseismic emissions at deeper levels," *International Journal of Rock Mechanics and Mining Sciences*, vol. 36, no. 7, pp. 941–948, 1999.

[18] M. Alber, R. Fritschen, M. Bischoff, and T. Meier, "Rock mechanical investigations of seismic events in a deep longwall coal mine," *International Journal of Rock Mechanics and Mining Sciences*, vol. 46, no. 2, pp. 408–420, 2009.

[19] J. He, L. Dou, S. Gong, J. Li, and Z. Ma, "Rock burst assessment and prediction by dynamic and static stress analysis based on micro-seismic monitoring," *International Journal of Rock Mechanics and Mining Sciences*, vol. 93, pp. 46–53, 2017.

[20] T.-H. Ma, C.-A. Tang, S.-B. Tang et al., "Rockburst mechanism and prediction based on microseismic monitoring," *International Journal of Rock Mechanics and Mining Sciences*, vol. 110, pp. 177–188, 2018.

[21] J. Y. Fan, W. Liu, D. Y. Jiang, W. N. Tiedeu, and J. J. K. Daemen, "Time interval effect in triaxial discontinuous cyclic compression tests and simulations for the residual stress in rock salt," *Rock Mechanics and Rock Engineering*, vol. 53, 2020.

[22] J. Cheng, Z. Wan, S. S. Peng, S. Liu, and Y. Ji, "What can the changes in shield resistance tell us during the period of shearer's cutting and neighboring shields' advance?" *International Journal of Mining Science and Technology*, vol. 25, no. 3, pp. 361–367, 2015.

[23] M. G. Qian, X. B. Mao, and X. X. Miao, "Variation of loads on the key layer of the overlying strata above the working," *Journal of China Coal Society*, vol. 23, no. 2, pp. 135–139, 1998.

[24] M. G. Qian, J. S. Yin, and S. Y. Liu, "Immediate roof caving in, tip to face , area of fully mechanized longwall face," *Journal of China Coal Society*, vol. 15, no. 1, pp. 1–9, 1990.

[25] X. X. Miao, X. B. Mao, and T. Z. Zhou, "Elastic foundation structure analysis of stope main roof and weighting forecast," *Mechanics in Engineering*, vol. 41, pp. 21-22, 1995.

[26] X. Y. Li, N. J. Ma, Y. P. Zhong, and Q. C. Gao, "Storage and release regular of elastic energy distribution in tight roof fracture," *Chinese Journal of Rock Mechanics and Engineering*, vol. 26, no. 1, pp. 2786–2793, 2007.

[27] K. S. Fan and B. H. Shen, "Research on mining thickness effect of underground mine pressure behavior by fully-mechanized caving mining in extra thick coal seams," *Coal Science and Technology*, vol. 47, no. 3, pp. 239–243, 2019.